Clinical Biomechanics

Submitted on April 5, 2005
Revised on October 18, 2005

ARTHROSCOPIC EVALUATION OF CARTILAGE DEGENERATION USING INDENTATION TESTING – INFLUENCE OF INDENTER GEOMETRY

L.P. Li * and **W. Herzog**

Faculty of Kinesiology, University of Calgary, Alberta, Canada

*Corresponding author:
LePing Li
Faculty of Kinesiology
University of Calgary
2500 University Drive, N.W.
Calgary, Alberta, Canada T2N 1N4

Email: leping@kin.ucalgary.ca

Abstract

Background. It has been suggested that the early onset of cartilage degeneration might be detected with a handheld indentation probe during knee arthroscopy, prior to any visible change on the articular surface. Collagen degradation has been considered as the first sign of cartilage degeneration. Therefore, it is important to consider the collagen network as a distinct constituent in the study of arthroscopic evaluation of cartilage degeneration.

Methods. The tip of an arthroscopic probe (indenter) was modeled as rigid and in contact with a cartilage/bone disk of sufficiently large radius to simulate an indentation in a joint. A fibril-reinforced model of cartilage, including streaming potentials and distinct constitutive laws for the proteoglycan matrix and collagen network, was used to determine the contact mechanics of indenter and cartilage. The finite element package ABAQUS was employed to obtain numerical solutions.

Findings. A spherical indenter produces a relatively uniform deformation in cartilage, but can easily slide on the articular surface. In contrast, a cylindrical indenter produces great deformation gradients for quick compression rates, but does not slide as easily on the articular surface as the spherical indenter. Small porous and large solid indenters should be used to evaluate the properties of the proteoglycan matrix and collagen network, respectively, in order to minimize or maximize the fluid pressure in the corresponding case. When the collagen network is substantially degraded, the gradients of fluid pressure and deformation are greatly reduced regardless of indenter geometry.

Interpretation. The indenter geometry including its porosity is important to the material safety of articular cartilage in indentation and precise evaluation of cartilage degeneration.

Keywords: Arthroscopic probe; Arthritis diagnosis; Articular cartilage mechanics; Cartilage degeneration; Fibril reinforced model; Indentation testing

1. INTRODUCTION

Indentation testing has been widely used to determine the mechanical properties of articular cartilage (Hayes et al., 1972; Kempson et al., 1971), including Poisson's ratios (Jin and Lewis, 2004), anisotropic properties (Bischoff, 2004), and electrochemical properties (Lu et al., 2004). Recently, it has been suggested that the early onset of cartilage degeneration may be detected with a handheld indentation probe during knee arthroscopy (Duda et al., 2004; Lyyra et al., 1995; Niederauer et al., 2004), prior to any visible signs of damage on the articular surface. Using manual compression with an arthroscopic probe to the articular surface of the knee, the load response and/or streaming potentials produced by the fluid pressure gradients have been measured (Garon et al., 2002, 2003). The corresponding results were associated with the Mankin score, a clinical indicator of the degree of cartilage degeneration (Franz et al., 2001; Mankin et al., 1971; van der Sluijs et al., 1992). In some applications, an ultrasound transducer was also integrated into the probe to obtain additional data (Hattori et al., 2003; Suh et al., 2001). Such arthroscopic probes have also been used to evaluate cartilage repair (Vasara et al., 2005).

An essential step of arthroscopic evaluation is to estimate the material properties of cartilage from the measured forces, pressures, strains or streaming potentials. Such estimates are possible with a theoretical model of contact between arthroscopic probe and cartilage surface. Typically, the results from indentation testing were interpreted using elastic or biphasic models in which material properties were not defined separately for the proteoglycan matrix and collagen network. Given the distinct roles of these two constituents in the load response and degeneration of articular cartilage (Aigner and Stöve, 2003; Mizrahi et al., 1986), we modeled the interaction between the arthroscopic indenter and articular cartilage using a fibril reinforced model in which the proteoglycan matrix and collagen network were represented with different material properties (Li et al., 1999). This model allows for differentiation between proteoglycan depletion and collagen digestion (Korhonen et al., 2003), and may give a better description of the

strain-rate dependent load response observed in experiments (Li and Herzog, 2004). Streaming potentials were also incorporated into the fibril reinforced model (Li and Herzog, 2005), because of their relevance in evaluating the integrity of articular cartilage (Grodzinsky et al., 1981; Gu et al., 1999; Kim et al., 1995; Légaré et al., 2002).

Fluid pressurization is a basic response of articular cartilage to loading. In arthroscopic indentation, the geometry of the indenter affects the pore fluid pressure in the contact region and the contact stresses. The objective of the present study was to explore the relevance of indenter shape, size and porosity in arthroscopic evaluation of articular cartilage using a fibril reinforced model. Differences in slip properties of spherical and cylindrical indenters were quantified, and the effect of indenter size and porosity on fluid pressurization was investigated.

2. METHODS

The tip of the arthroscopic probe was considered rigid (porous or non-porous), and in contact with a cartilage/bone disk of sufficiently large radius to simulate an arthroscopic indentation in a joint. Preliminary calculations showed that deformation and stresses for the loading conditions and indention geometry considered here were confined to the vicinity of the contact region, and thus a radius of 6mm was sufficient to cover the loaded region. Axisymmetry was assumed in all analyses, and the effects of bone deformation on the load response were found to be negligible. Therefore, the tissue disk was modeled as a cartilage layer of 1.13mm bonded to a rigid substrate. The maximum compression applied by the indenters was limited to 200μm. The loading speed was 200μm/s except for one case in which a lower compression speed was simulated for evaluation of rate effects.

Spherical and cylindrical indenter geometries were simulated. Cylindrical, plane-ended indenters are commonly used in experiments (Mow et al., 1989; Suh and Spilker, 1994; Zhang et al., 1997). We also considered a spherical indenter with the same geometry as the Arthro-BST^{TM}

probe (Biosyntech Inc., Montreal, Canada) which is instrumented with microelectrodes for detection of streaming potentials. The spherical indenter was modeled with a radius of 4.20mm, the cylindrical indenter with a radius of 1.25mm (default) or 0.50mm for evaluation of size effects.

Finite element solutions were obtained using the surface-based contact approach formulated in ABAQUS/Standard (ABAQUS Inc., Providence, USA). The problem was defined by the contact between a rigid master surface (tip of probe) and a deformable slave surface (articular surface). The nodes of the slave surface were constrained not to penetrate into the master surface, which was enforced by Lagrange multiplier techniques. Sufficient nodes were meshed to obtain a smooth surface deformation (Figs. 1, 2 & 7, nodes of the 8-node elements). The "small sliding" option was used for rapid convergence, which was justified as it was assumed that the probe did not slide on the articular surface (i.e. no rigid movement of the probe on the articular surface was simulated). The geometrical nonlinearity option was activated for all analyses.

The coefficient of friction (f) between indenter and articular surface was varied from 0 to 0.15, in reference to the measured macroscale coefficients ranging from 0.004 at transient to 0.138 at equilibrium (Park et al., 2004). However, larger coefficients of friction were also considered for cases in which fibril reinforcement was absent, representing the theoretical limit of collagen degeneration (Fig. 6 only).

Articular cartilage was modeled with strain and direction dependent collagen fibrillar moduli, Young's modulus (0.26MPa) and Poisson's ratio (0.36) of the nonfibrillar proteoglycan matrix, as well as permeability ($0.003\text{mm}^4/\text{Ns}$), conductivity and the electrokinetic coupling parameters (Li and Herzog, 2005). Streaming potentials were not investigated in the present study, and thus the values for conductivity and coupling parameters were not required. The fibrillar moduli in the radial and axial directions were, respectively, $(3+1600\varepsilon_r)$ and $(1.5+800\varepsilon_z)$

MPa, with the exception of Fig. 6, where the fibrillar stiffness was neglected to simulate a severe collagen breakdown. The void ratio was taken to be 3.5.

3. RESULTS

The deformation produced by the spherical indenter was quite uniform even at the edge of the contact region, and the numerical results were satisfactory even with a relatively coarse mesh (Fig. 1). In contrast, the deformations produced by the cylindrical indenters were large and highly non-uniform at the edge of the contact region (Fig. 2). For the case with a fillet radius (r_f) of 0.05mm (Fig. 2a), the solution failed to converge after 0.488s even with a refined mesh. For the case with a fillet radius of 0.10mm (Fig. 2b), numerical solutions were obtained up to around 0.7s (shown for 0.5s).

Frictions at the contact surface had a negligible effect on the total reaction force on the indenter or the vertical load on cartilage. For example, the vertical reaction force on the spherical indenter at 1s (200μm compression) was increased only by 1.4% (from 16.92 to 17.16N) when the coefficient of friction was increased from 0 to 0.15 (not shown).

Friction at the contact surface was produced by the lateral expansion of cartilage when compression was applied perpendicularly to the articular surface, even if no lateral sliding of the indenter occurred. The load applied to the indenter was therefore balanced by the friction and contact pressure (total normal stress) from the articular cartilage. A free body diagram of the indenter in the axisymmetric model is shown in the inset of Fig. 3 (vertical forces are not specified). The variables F_f and F_p are, respectively, identical to the scalar integrals of the horizontal components of friction and contact pressure (ABAQUS output). The vectorial resultants of the horizontal components are actually zero if the indenter does not slip. However, F_f is a measure of the friction force in the event of indenter slipping.

F_f increased quickly with the coefficient of friction at small f and reached its asymptotic value at approximately 0.15 (Fig. 3 for the spherical indenter, the asymptotic response is not shown; Fig. 4 for the cylindrical indenter, the asymptotic response is shown in the inset). F_p on the spherical indenter at 1s (200μm compression) was increased only by 4.8% from 2.49 to 2.61N when f was changed from 0 to 0.15 (not shown). The influence of friction on F_p for the cylindrical indenter (with r_f = 0.10mm, Fig. 2b) was similar to that for the spherical indenter. However, the magnitude of F_p for the cylindrical indenter was considerably larger. For example, F_p was 0.238 and 0.316N (33% greater), respectively, for the spherical and cylindrical indenters at 0.5s (100μm compression) when friction was absent (not shown).

For the spherical indenter, F_p was always significantly greater than F_f. For the cylindrical indenter, however, $F_p - F_f < 0$ before the compression reached a certain level depending on f (Fig. 5). Since F_p changed little with altered f, this result demonstrates that friction plays a more important role in the cylindrical than spherical indenters.

When simulating osteoarthritic cartilage in which the collagen fiber network is degraded, the contact pressure was low for a given compression, resulting in low values of friction (Fig. 6). However, the asymptotic value for F_f was reached at a larger coefficient of friction ($f > 0.3$) in the osteoarthritic compared to the normal ($f \approx 0.15$) articular cartilage. Numerical solutions were possible for all cases reaching 200μm compression because of the relatively uniform deformation associated with the low fluid pressure in the contact regions (in contrast to the cases shown in Fig. 2).

When a solid indenter was replaced by a porous indenter of identical size (1.0mm in diameter), the fluid pressure was greatly altered (Fig. 7, for normal cartilage), resulting in a lower reaction force on the porous indenter. The vertical strain was relatively uniform in the case of solid indenter (Fig. 7a), while highly concentrated in the contact layer in the case of

porous indenter because low fluid pressure there made it easier for compression than the deeper layers (Fig. 7b).

4. DISCUSSION

The actual compression rate of the hand-held probe can be determined using a spherical indenter with a sufficient number of microelectrodes embedded in the tip. When an electrode located at point A is not in contact with the articular surface (Fig. 1a), no increment in streaming potential is detected. As soon as point A gets in contact with the articular surface (Fig. 1b), an increment in streaming potential is measured. Thus, the times when given locations at different radii begin to contact the tissue are recorded, and can be used to estimate the compression rate. Knowing the compression rate is important because the load response of articular cartilage is highly strain-rate dependent (Li and Herzog, 2004). Obviously, this approach can not be used with a flat-ended tip, such as that of a cylindrical indenter, to estimate the compression rate.

For a given amount of compression, a spherical indenter produces lower deformation gradients in the tissue than a cylindrical indenter (Fig. 1 vs. Fig. 2). Indenters with sharp edges ($r_f \approx 0$, defined in Fig. 2b) should not be used in order to avoid tissue damage. For the problem considered here, an indenter with a fillet of (r_f =) 0.05mm (Fig. 2a) might cause tissue matrix damage at a compression of 200μm. Increasing the fillet radius from 0.05 to 0.10mm resulted in considerably more uniform tissue deformations, whereas this effect became less significant for large fillet radii (calculated up to r_f = 0.40mm, not shown). Therefore, a fillet radius of 0.10mm may be appropriate for the loading conditions discussed here (Fig. 2b).

The cylindrical indenter does not slip as easily on the articular surface as the spherical indenter. In an arthroscopic evaluation, it is hard to apply a force perfectly perpendicular to the articular surface. Lateral forces may result in a sliding of the probe on the surface. The results obtained with no probe sliding may be served as a reference for evaluation of probe sliding: a

larger F_f (Fig. 3 inset) means a smaller possibility of (continuous) sliding, which is the case for the cylindrical indenter.

It has been reported that the load does not increase significantly with the friction coefficient, once $f > 0.3$ in an elastic model (no fluid flow) with a cylindrical indenter (Zhang et al., 1997). This result is similar to what is predicted by our model (with fluid flow) for osteoarthritic cartilage (Fig. 6, load not shown). The asymptotic response was reached at a smaller f (≈ 0.15) for normal cartilage in the presence of fibril reinforcement (Fig. 4 inset). In addition, high fluid pressures and great local strains are all associated with fibril reinforcement.

The size of the larger cylindrical indenter used in our simulations (2.5mm in diameter) was still within the range used in cartilage indentation (Spoon and Wayne, 2004), but was larger than indenters used in some other studies (1.5mm: Mow et al., 1989; Suh and Spilker, 1994; 0.8mm: Korhonen et al., 2002). Previous studies have shown that fluid pressure in cartilage is mainly associated with the nonlinear properties of the collagen network that makes little contribution to the equilibriums response (Li et al., 1999; Li and Herzog, 2004). Here, we used a larger nonporous indenter to ensure good fluid pressurization in the contact region so that collagen degradation could be evaluated more sensitively than with a smaller indenter.

The properties of the proteoglycan matrix should be evaluated at equilibrium, or at the lowest fluid pressure possible, in order to minimize the contribution of collagen network to the load response of cartilage. Reducing the compression rate can effectively lower fluid pressure: the transient load, mostly supported by fluid pressure, was reduced from 10.81 (44.50× equilibrium load, case shown in Fig. 2b) to 0.93N (3.82× equilibrium load, not shown) for a compression of 100μm, when the rate was reduced from 200 to 1μm/s. However, the duration for load application by hand must be minimized. Reducing the indenter size and using a porous indenter are additional measures that can be used to lower fluid pressure during arthroscopic evaluation (Fig. 7). For a compression of 100μm applied at 200μm/s, the transient load was

reduced from 44.5 times of its equilibrium load (10.81N/0.2429N) to 21.5 times of its new equilibrium load (1.148N/0.0533N), when the diameter of a solid indenter was reduced from 2.5 to 1.0mm.

The transient load was further reduced by making the indenter ideally permeable. For the smaller indenter (1.0mm in diameter), the load was reduced by 40% (from 0.539 to 0.326N) at a compression of 60μm (5.3% of the tissue thickness) applied at 200μm/s, if a solid indenter was replaced by a porous indenter (cases shown in Fig. 7). It was reported that the load was only reduced by approximately 10% due to such replacement, when a displacement of 10% of the tissue thickness was applied in 500s (Spilker et al., 1992). The influence of indenter porosity was much greater in our case mainly because of the high compression rate considered and the ability of our model to approximate fast compression.

The collagen network was assumed to be nonlinearly elastic in the present study. While collagen fibers are known to be viscoelastic, stress relaxation in fibers was found to have a negligible effect on the load response of cartilage in fast unconfined compression, as long as the fibrillar moduli were defined as the instantaneous Young's moduli of the network (Li et al., 2005). This finding should also apply to the indentation analyses presented here, because the time involved for compression was short (≤ 1s except for one case used for comparison).

The axisymmetric modeling used here poses some limitations. The potential rigid movement of a probe on the articular surface was not simulated. Instead, possible probe sliding was assessed by the total friction obtained for the probe with no lateral movement. Accounting for the fiber orientation in the split direction also requires three-dimensional modeling. In addition, the constitutive laws used for cartilage may need to be revised to accommodate very large deformations, in order to improve the accuracy and convergence of the results for problems with great local strains as may occur in the case of some cylindrical indenters (Fig. 2).

In conclusion, a spherical indenter produces more uniform strains and appears safer for cartilage indentation. A cylindrical indenter produces highly non-uniform strains at high-speed compression, but is less likely to slide on the articular surface. Small porous and large solid indenters should be used to approximate, respectively, the equilibrium and instantaneous responses of articular cartilage so that the properties of the proteoglycan matrix and collagen network may be evaluated effectively. The equilibrium strains are much more uniform than the transient strains for the spherical and cylindrical indenters. Therefore, a very small fillet for the cylindrical indenter would be sufficient for evaluating the proteoglycan matrix. Using a cylindrical indenter with a fillet of sufficiently large radius is suggested for evaluating the collagen network. Finally, the results presented here are associated with collagen fibril reinforcement that determines the transient load response of normal or degenerative articular cartilage. We would have concluded differently if fibril reinforcement had not been considered.

ACKNOWLEDGEMENTS

This study was supported by the Canadian Institutes of Health Research and the Canada Research Chair Program.

REFERENCES

Aigner, T., Stöve, J. (2003) Collagens – major component of the physiological cartilage matrix, major target of cartilage degeneration, major tool in cartilage repair. *Advanced Drug Delivery Reviews* **55**, 1569-1593.

Bischoff, J.E. (2004) Static indentation of anisotropic biomaterials using axially asymmetric indenters – a computational study. *ASME Journal of Biomechanical Eng* **126**, 498-505.

Duda, G.N., Kleemann, R.U., Bluecher, U., Weiler, A. (2004) A new device to detect early cartilage degeneration. *American Journal of Sports Medicine* **32**, 693-698.

Franz, T., Hasler, E.M., Hagg, R., Weiler, C., Jakob, R.P., Mainil-Varlet, P. (2001) In situ compressive stiffness, biochemical composition, and structural integrity of articular cartilage of the human knee joint. *Osteoarthritis and Cartilage* **9**, 582-592.

Garon, M., Légaré, A., Guardo, R., Savard, P., Buschmann, M.D. (2002) Streaming potentials maps are spatially resolved indicators of amplitude, frequency and ionic strength dependant responses of articular cartilage to load. *Journal of Biomechanics* **35**, 207-216.

Garon, M., Légaré, A., Quenneville, E., Hurtig, M.B., Buschmann, M.D. (2003) Streaming potential based arthroscopic instrument distinguishes site-specific properties of equine articular cartilage. *Transactions of the Orthopaedic Research Society* **28**, 255.

Grodzinsky, A.J., Roth, V., Myers, E., Grossman, W.D., Mow, V.C. (1981) The significance of electromechanical and osmotic forces in the nonequilibrium swelling behavior of articular cartilage in tension. *ASME Journal of Biomechanical Engineering* **103**, 221-230.

Gu, W.Y., Mao, X.G., Rawlins, B.A., Iatridis, J.C., Foster, R.J., Sun, D.N., Weidenbaum, M., Mow, V.C. (1999) Streaming potential of human lumbar annulus fibrosus is anisotropic and affected by disc degeneration. *Journal of Biomechanics* **32**, 1177-1182.

Hattori, K., Mori, K., Habata, T., Takakura, Y., Ikeuchi, K. (2003) Measurement of the mechanical condition of articular cartilage with an ultrasonic probe: quantitative evaluation using wavelet transformation. *Clinical Biomechanics* **18**, 553-557.

Hayes, W.C., Keer, L.M., Herrmann, G., Mockros, L.F. (1972) A mathematical analysis for indentation tests of articular cartilage. *Journal of Biomechanics* **5**, 541-551.

Jin, H., Lewis, J.L. (2004) Determination of Poisson's ratio of articular cartilage by indentation using different-sized indenters. *ASME Journal of Biomechanical Engineering* **126**, 138-145.

Kempson, G.E., Freeman, M.A.R., Swanson, S.A.V. (1971) The determination of a creep modulus for articular cartilage from indentation tests on the human femoral head. *Journal of Biomechanics* **4**, 239-250.

Kim, Y.J., Bonassar, L.J., Grodzinsky, A.J. (1995) The role of cartilage streaming potential, fluid flow and pressure in the stimulation of chondrocyte biosynthesis during dynamic compression. *Journal of Biomechanics* **28**, 1055-1066.

Korhonen, R.K., Laasanen, M.S., Töyräs, J., Lappalainen, R., Helminen, H.J., Jurvelin, J.S. (2003) Fibril reinforced poroelastic model predicts specifically mechanical behavior of normal, proteoglycan depleted and collagen degraded articular cartilage. *Journal of Biomechanics* **36**, 1373-1379.

Korhonen, R.K., Wong, M., Arokoski, J., Lindgren, R., Helminen, H.J., Hunziker, E.B., Jurvelin, J.S. (2002) Importance of the superficial tissue layer for the indentation stiffness of articular cartilage. *Medical Engineering & Physics* **24**, 99-108.

Légaré, A., Garon, M., Guardo, R., Savard, P., Poole, A.R., Buschmann, M.D. (2002) Detection and analysis of cartilage degeneration by spatially resolved streaming potentials. *Journal of Orthopaedic Research* **20**, 819-826.

Li, L.P., Herzog, W. (2004) Strain-rate dependence of cartilage stiffness in unconfined compression: the role of fibril reinforcement versus tissue volume change in fluid pressurization. *Journal of Biomechanics* **37**, 375-382.

Li, L.P., Herzog, W. (2005) Electromechanical response of articular cartilage in indentation – Considerations on the determination of cartilage properties during arthroscopy. *Computer Methods in Biomechanics and Biomedical Engineering* **8**, 83-91.

Li, L.P., Herzog, W., Korhonen, R.K., Jurvelin, J.S. (2005) The role of viscoelasticity of collagen fibers in articular cartilage: axial tension versus compression. *Medical Engineering & Physics* **27**, 51-57.

Li, L.P., Soulhat, J., Buschmann, M.D., Shirazi-Adl, A. (1999) Nonlinear analysis of cartilage in unconfined ramp compression using a fibril reinforced poroelastic model. *Clinical Biomechanics* **14**, 673-682.

Lu, X.L., Sun, D.D.N., Guo, X.E., Chen, F.H., Lai, W.M., Mow, V.C. (2004) Indentation determined mechanoelectrochemical properties and fixed charge density of articular cartilage. *Annals of Biomedical Engineering* **32**, 370-379.

Lyyra, T., Jurvelin, J., Pitkänen, P., Väätäinen U., Kiviranta, I. (1995) Indentation instrument for the measurement of cartilage stiffness under arthroscopic control. *Medical Engineering & Physics* **17**, 395-399.

Mankin, H.J., Dorfman, H., Lippiello, L., Zarins, A. (1971) Biochemical and metabolic abnormalities in articular cartilage from osteoarthritic human hips. *Journal of Bone and Joint Surgery* **53A**, 523-537.

Mizrahi, J., Maroudas, A., Lanir, Y., Ziv, I., Webber, T.J. (1986) The "instantaneous" deformation of cartilage: effects of collagen fiber orientation and osmotic stress. *Biorheology* **23**, 311-330.

Mow, V.C., Gibbs, M.C., Lai, W.M., Zhu, W.B., Athanasiou, K.A. (1989) Biphasic indentation of articular cartilage – II. A numerical algorithm and an experimental study. *Journal of Biomechanics* **22**, 853-861.

Niederauer, G.G., Niederauer, G.M., Cullen, L.C. Jr., Athanasiou, K.A., Thomas, J.B., Niederauer, M.Q. (2004) Correlation of cartilage stiffness to thickness and level of degeneration using a handheld indentation probe. *Annals of Biomedical Eng* **32**, 352-359.

Park, S., Costa, K.D., Ateshian, G.A. (2004) Microscale frictional response of bovine articular cartilage from atomic force microscopy. *Journal of Biomechanics* **37**, 1679-1687.

Spilker, R.L., Suh, J.K., Mow, V.C. (1992) A finite element analysis of the indentation stress-relaxation response of linear biphasic articular cartilage. *ASME Journal of Biomechanical Engineering* **114**, 191-201.

Spoon, C.E., Wayne, J.S. (2004) Influence of aspect ratios on the creep behaviour of articular cartilage in indentation. *Computer Methods in Biomechanics and Biomedical Eng* **7**, 17-23

Suh, J.K., Spilker, R.L. (1994) Indentation analysis of biphasic articular cartilage: nonlinear phenomena under finite deformation. *ASME Journal of Biomechanical Engineering* **116**, 1-9.

Suh, J.K.F., Youn, I., Fu, F.H. (2001) An in situ calibration of an ultrasound transducer: a potential application for an ultrasonic indentation test of articular cartilage. *Journal of Biomechanics* **34**, 1347-1353.

van der Sluijs, J.A., Geesink, R.G.T., van der Linden, A.J., Bulstra, S.K., Kuyer, R., Drukker, J. (1992) The reliability of the Mankin score for osteoarthritis. *Journal of Orthopaedic Research* **10**, 58-61.

Vasara, A.I., Nieminen, M.T., Jurvelin, J.S., Peterson, L., Lindahl, A., Kiviranta, I. (2005) Indentation stiffness of repair tissue after autologous chondrocyte transplantation. *Clinical Orthopaedics & Related Research* **433**, 233-242.

Zhang, M., Zheng, Y.P., Mak, A.F.T. (1997) Estimating the effective Young's modulus of soft tissues from indentation tests – nonlinear finite element analysis of effects of friction and large deformation. *Medical Engineering & Physics* **19**, 512-517.

FIGURE CAPTIONS

Fig. 1 Transient deformation of cartilage in the contact region, at 100 and 200μm compression (Figures a and b respectively) applied by a spherical indenter at a speed of 200μm/s. The indenter was considered rigid and impervious with a radius of 4.20mm. The friction between the indenter and tissue was neglected. The radius of the tissue disk was 6.00mm, with cartilage thickness being 1.13mm. The underlying bone was assumed to be rigid. The finite element mesh for the axisymmetric problem was 32×12, with thirty-two 8-node elements of different size in the radial direction, and twelve elements evenly distributed in the axial direction. For clarity of the figure, only part of the mesh is shown (half cartilage thickness, radius 2.00mm in original size; all elements shown were identical before deformation).

Fig. 2 Transient deformation of cartilage in the outer contact region (0.375mm < r ≤ 1.750mm, half cartilage thickness; r is the radial coordinate), with compression applied by a cylindrical indenter of radius 1.25mm. The edge of the indenter tip was smoothed with a fillet of radius r_f . The mesh around the edge of the indenter was refined to half the height and half the width, compared to the mesh shown in Fig. 1. Other conditions were the same as those for the case shown in Fig. 1. a) for a compression of 97.6μm (at time 0.488s), r_f = 0.05mm; b) for a compression of 100μm (at time 0.500s), r_f = 0.10mm.

Fig. 3 Horizontal friction force (F_f) on the spherical indenter, for the case shown in Fig. 1 after a constant coefficient of friction (f) was introduced. The inset shows all horizontal forces acting on the indenter: F_f and F_p are, respectively, the total friction and contact pressure between the indenter and tissue in the horizontal direction, and F_o is the horizontal reaction force that balances F_f and F_p. These quantities are the variables in finite element modeling for the axisymmetric problem.

Fig. 4 Horizontal friction force (F_f) on the cylindrical indenter, for the case shown in Fig. 2b (r_f = 0.10mm) after a constant coefficient of friction (f) was introduced. The horizontal forces (F_o , F_f and F_p) on the cylindrical indenter were defined similarly to those on the spherical indenter as shown in the inset of Fig. 3. The inset in this figure shows the friction force as a function of the coefficient, at 0.5 seconds or at a compression of 100μm (calculated for the following friction coefficients: 0.01, 0.03, 0.05, 0.07, 0.10, 0.12, 0.15 and 0.20).

Fig. 5 Horizontal reaction force (F_o, or $F_p - F_f$, as shown in the inset of Fig. 3) on the cylindrical indenter shown in Fig. 2b (r_f = 0.10mm), for the cases shown in Fig. 4 with inclusion of frictionless contact (f = 0). It was assumed that the indenter did not experience any lateral rigid movement.

Fig. 6 Horizontal friction force (F_f , as shown in the inset of Fig. 3) on the spherical or cylindrical indenter as a function of the coefficient of friction (f), in absence of fibril reinforcement, shown for compression magnitudes of 100 and 200μm. Other conditions were the same as those for the case shown in Fig. 1 for the spherical indenter or Fig. 2b for the cylindrical indenter, where fibril reinforcement was considered.

Fig. 7 Pore fluid pressure (MPa) in the contact region, at 60μm compression applied at 200μm/s, upon application of solid and porous indenters, shown in Figures a) and b) respectively. Both indenters are cylindrical of radius 0.50mm and fillet radius 0.10mm. The indenters were considered rigid undergoing frictionless contact with the tissues. The mesh is 30×12 for the region shown (dimension: 0.75mm × 1/4 cartilage thickness of 1.13mm). The maximum fluid pressure occurred at the contact center for the case of a solid indenter; it occurred at a depth of approximately 0.06mm for the case of a porous indenter (marked with asterisks).

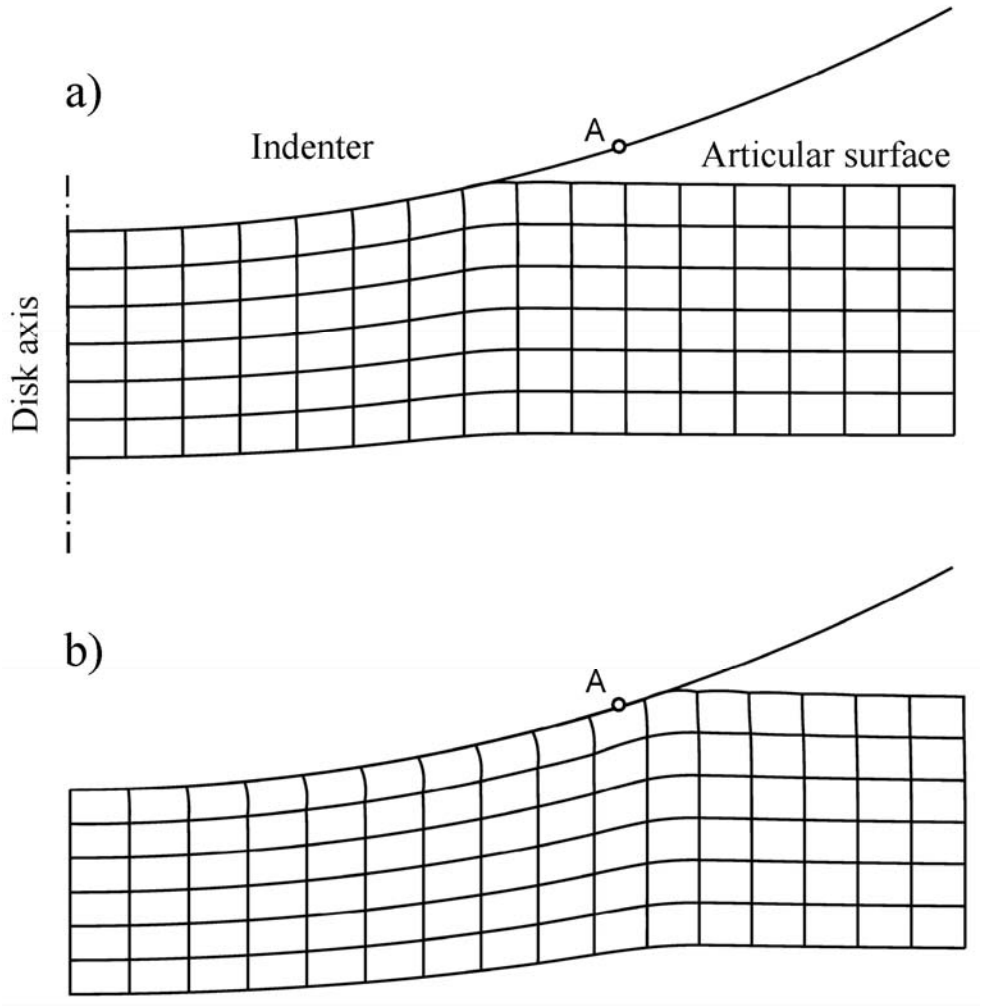

Figure 1

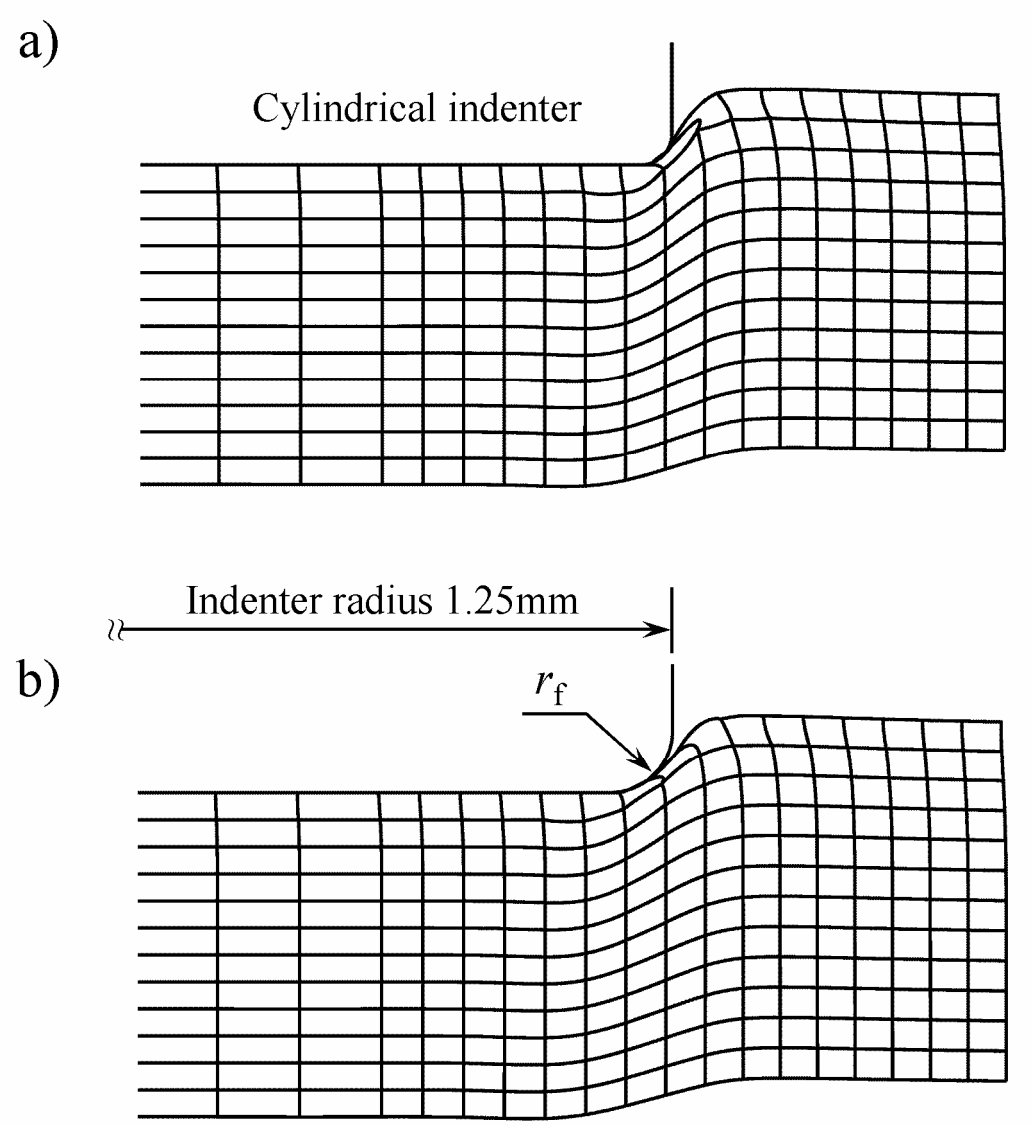

Figure 2

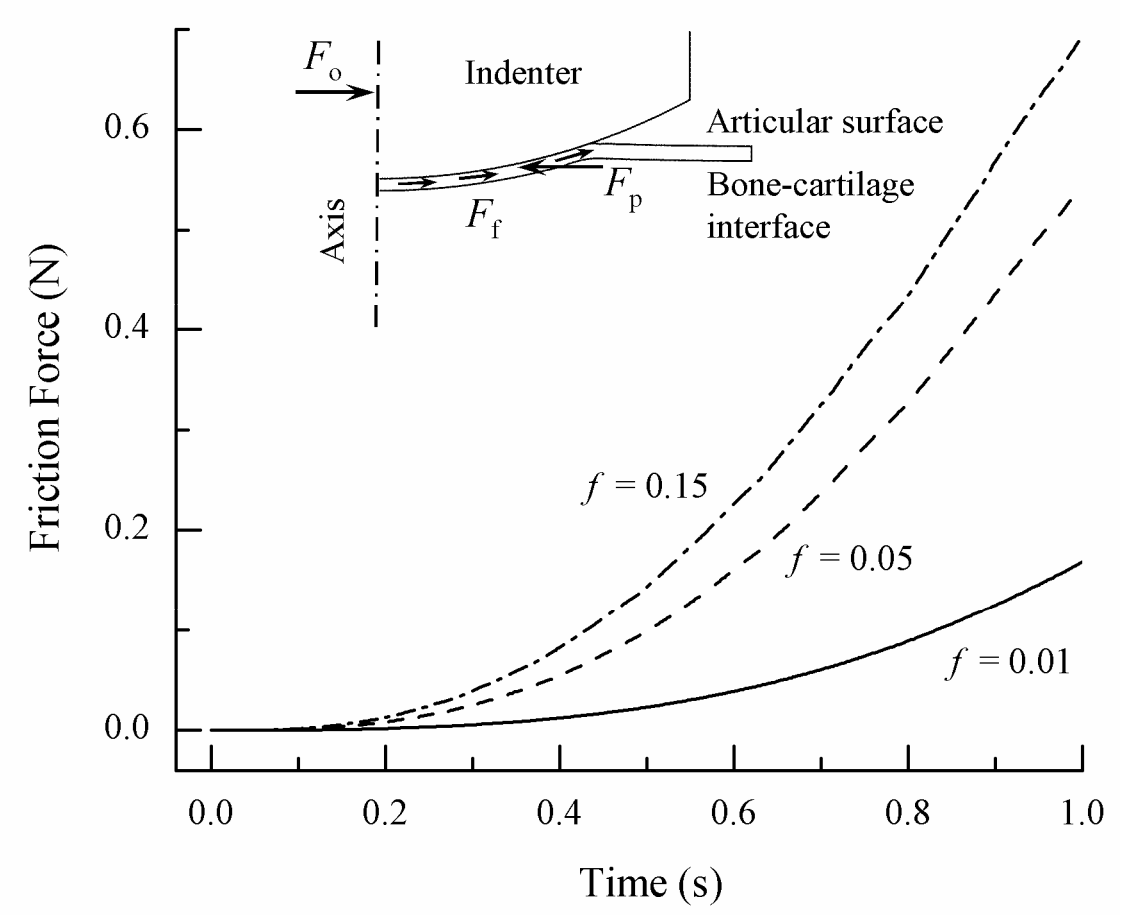
F_o
Indenter
Articular surface
F_p
Bone-cartilage interface
F_f
Axis
Friction Force (N)
0.0
0.2
0.4
0.6
f = 0.15
f = 0.05
f = 0.01
0.0
0.2
0.4
0.6
0.8
1.0
Time (s)

Figure 3

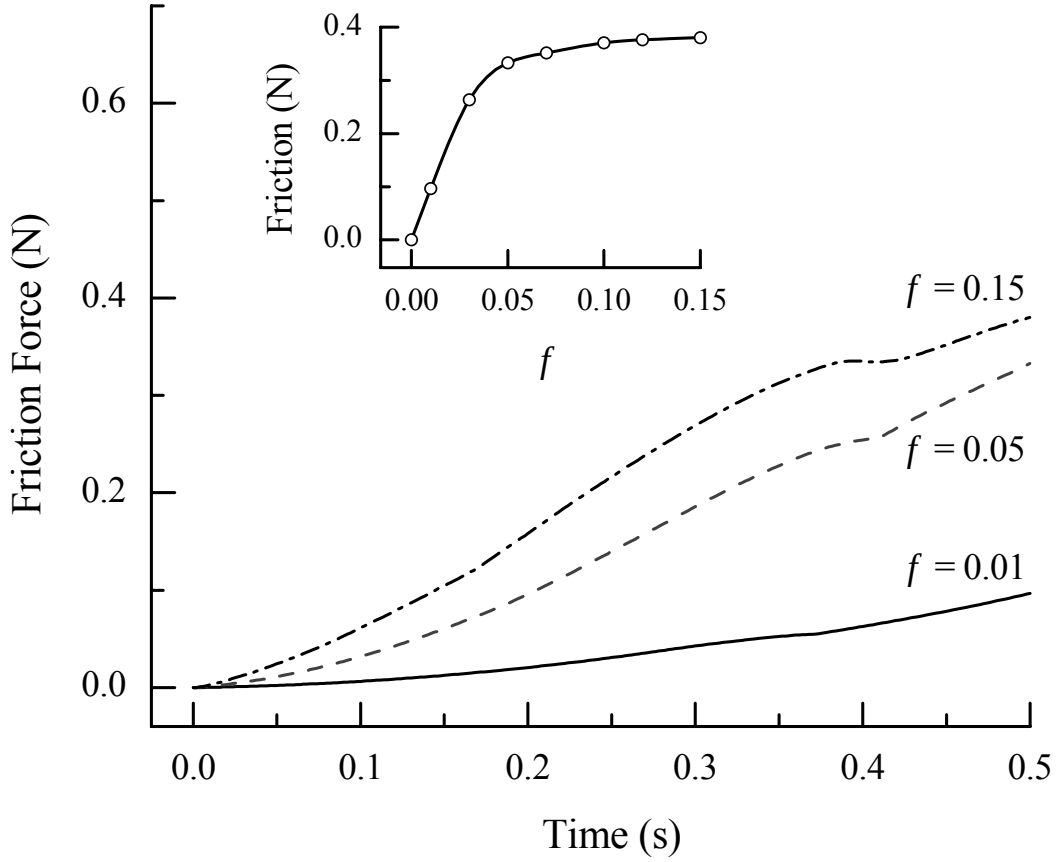
Friction Force (N)
0.0
0.2
0.4
0.6
0.0
0.1
0.2
0.3
0.4
0.5
Time (s)
f = 0.15
f = 0.05
f = 0.01
Friction (N)
0.0
0.2
0.4
0.00
0.05
0.10
0.15
f

Figure 4

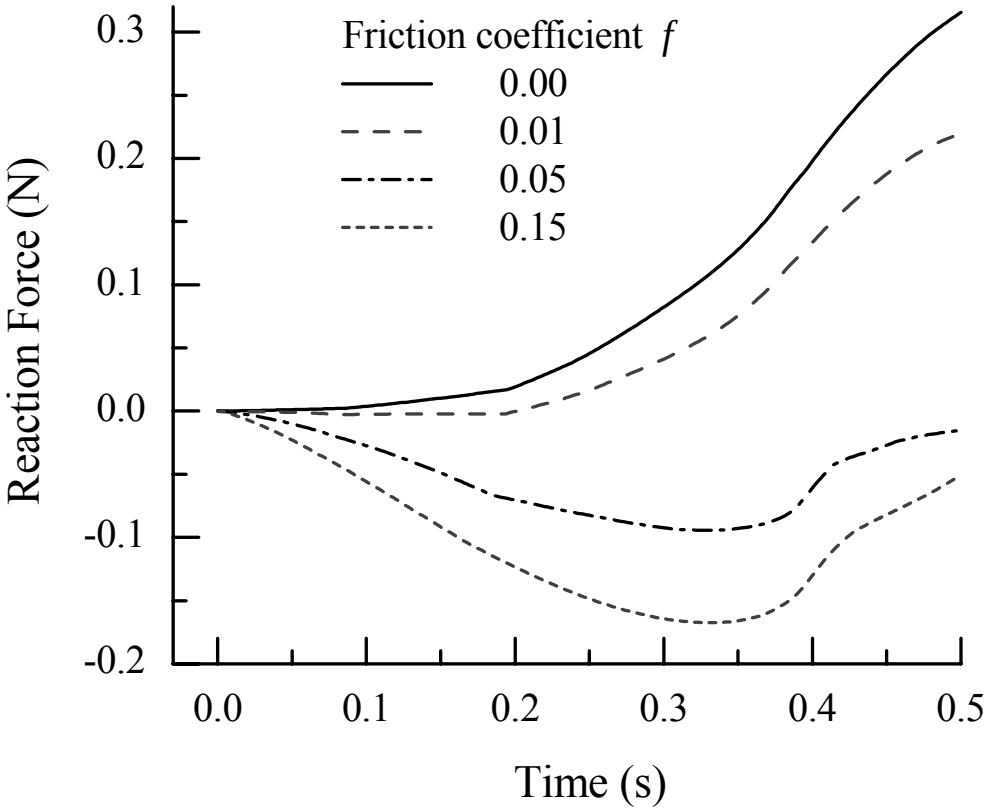
Friction coefficient f
0.00
0.01
0.05
0.15
Reaction Force (N)
0.3
0.2
0.1
0.0
-0.1
-0.2
0.0
0.1
0.2
0.3
0.4
0.5
Time (s)

Figure 5

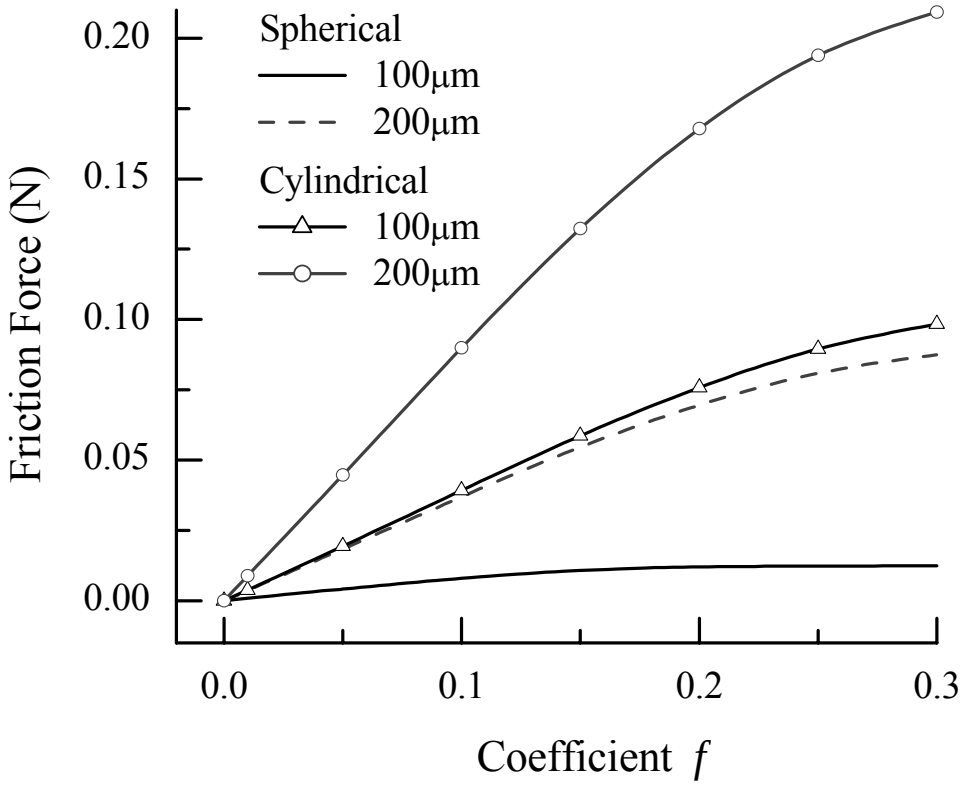
Spherical
100μm
200μm
Cylindrical
100μm
200μm
Friction Force (N)
0.20
0.15
0.10
0.05
0.00
0.0
0.1
0.2
0.3
Coefficient f

Figure 6

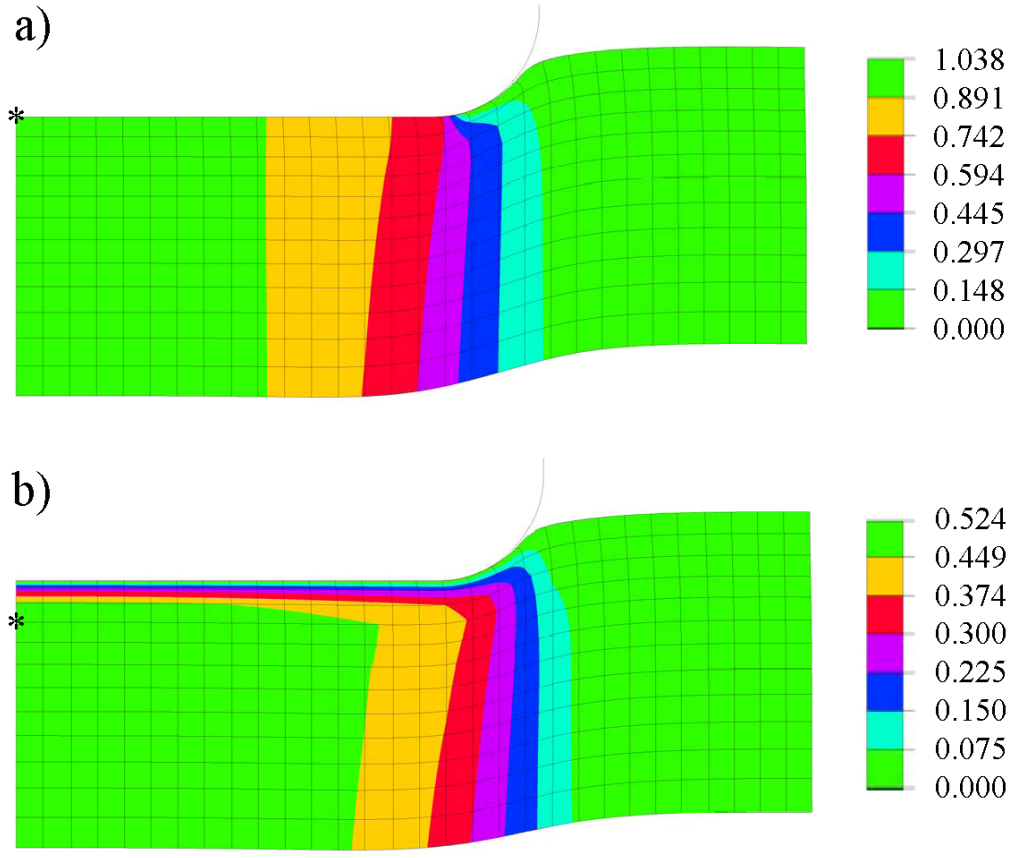
a)
*
1.038
0.891
0.742
0.594
0.445
0.297
0.148
0.000
b)
*
0.524
0.449
0.374
0.300
0.225
0.150
0.075
0.000

Figure 7